Apatite Crystallization in an Aluminosilicate Glass Matrix: Mechanistic Studies by X-ray Powder Diffraction, Thermal Analysis, and Multinuclear Solid-State NMR Spectroscopy

Jerry C. C. Chan, Richard Ohnsorge, Karin Meise-Gresch, and Hellmut Eckert*

Institut für Physikalische Chemie, Westfälische Wilhelms-Universität Münster, Schlossplatz 7, D-48149 Münster, Germany

Wolfram Höland and Volker Rheinberger

Ivoclar, Ltd., FL-9494 Schaan, Principality of Liechtenstein

Received February 28, 2001. Revised Manuscript Received July 27, 2001

The crystallization of fluoroapatite, $Ca_5(PO_4)_3F$ (FAP), from a phase-separated glass of composition (mol %) 61.5 SiO_2−9.4 Al_2O_3−9.2 Na_2O−7.7 K_2O−6.0 CaO−1.9 P_2O_5−2.5 F, with minor additional components of CeO_2, ZrO_2, TiO_2, Li_2O, and B_2O_3, was monitored by X-ray powder diffraction (XRD), differential thermal analysis (DTA), and advanced high-resolution solid-state NMR spectroscopic techniques on two series of bulk and powder samples subjected to different annealing protocols. The chemical changes occurring as a function of heating time and temperature are sensitively reflected in the ^{31}P and ^{19}F magic-angle spinning (MAS) NMR spectroscopic results. Furthermore, important information concerning the elemental distribution over the two microphases and the chemical identity of crystallization intermediates can be revealed by various $^{31}P \leftrightarrow {}^{19}F$, $^{19}F \leftrightarrow {}^{27}Al$, $^{31}P \leftrightarrow {}^{23}Na$, $^{31}P \leftrightarrow {}^{27}Al$, and $^{23}Na \leftrightarrow {}^{19}F$ double-resonance NMR experiments. The glassy material separates into an aluminosilicate-type matrix glass and a droplet phase containing Ca, Na, and the entire phosphorus component. Fluorine dissolves in both of these phases, and the corresponding local environments are differentiable on the basis of their ^{19}F NMR chemical shifts and $^{19}F-{}^{31}P$ and $^{19}F-{}^{27}Al$ dipole−dipole coupling strengths. During the course of the crystallization, $^{31}P \leftrightarrow {}^{23}Na$ and $^{31}P \leftrightarrow {}^{19}F$ double-resonance NMR results confirm conclusions based on X-ray powder diffraction that the initial stages of crystallization involve the formation of fluorine-free precursor phases such as $NaCaPO_4$ and a sodium calcium phosphate silicate. However, the comparison between the two series indicates that the crystallization mechanism is also influenced by sample thermal history. Crystallization of fluoroapatite sets in at 700 °C as clearly revealed by XRD and double-resonance NMR. The results illustrate the utility of advanced solid-state NMR techniques for the study of crystallization processes in compositionally complex ceramics.

Introduction

The development of glass ceramics for useful applications as biomaterials for dental restoration requires strict control not only of the chemical composition but also of the shape, the morphology, and the mode of interpenetration of the various crystalline and glassy phases involved. Recent work has shown that the formation of needlelike apatite, an important biomaterial, can be controlled by crystallization from a phase-separated glassy precursor.[1] In essence, fluoroapatite, $Ca_5(PO_4)_3F$ (FAP), is precipitated from a droplet phase within a phase separated glass in the $SiO_2-Al_2O_3-K_2O-Na_2O-CaO-P_2O_5-F$ system. This crystallization process has been studied in detail, using scanning electron microscopy, X-ray powder diffraction, and various complementary analytical techniques.[2] In the course of these studies, X-ray powder diffraction results have suggested that apatite crystallization is preceded by the formation of a crystalline precursor phase of composition $NaCaPO_4$ and potentially a second, yet unidentified, crystalline material ("X-phase"). At the present time, it is unclear whether apatite forms via a heterogeneous reaction of the primary $NaCaPO_4$ crystals with the surrounding glassy matrix or whether the process is rather described by a reaction at the interfaces between the two glassy phases. Issues that remain to be resolved include (1) the distribution of phosphate and fluoride over the two distinct microphases in the glassy precursor material, (2) the local coordination environments

* To whom correspondence should be addressed.

(1) Höland, W.; Frank, M.; Schweiger, M.; Rheinberger, V. *Glass Sci. Technol. (Frankfurt/Main)* **1994**, *C67*, 117.

(2) (a) Höland, W.; Rheinberger, V.; Frank, M. *J. Non-Cryst. Solids* **1999**, *253*, 170. (b) Höche, T.; Moisescu, C.; Rüssel, C.; Heerdegen, W. D. *Glass Sci. Technol. (Frankfurt/Main)* **2000**, *73*, C1, 119. (c) Höland, W.; Schweiger, M.; Cramer von Clausbruch, S.; Rheinberger, V. *Glass Sci. Technol. (Frankfurt/Main)* **2000**, *73*, C1, 12.

10.1021/cm0101834 CCC: $20.00
Published on Web 10/18/2001

Table 1. Sample Heat Treatment Conditions and Phase Composition Determined from XRD

series I	phases	series II	main phases
(A) 400 °C/15 min	$Na_2Ca_4(PO_4)_2SiO_4$	(A) 500 °C/1 min	$NaCaPO_4$, SiO_2
(B) 580 °C/15 min	$Na_2Ca_4(PO_4)_2SiO_4$	(B) 550 °C/1 min	$NaCaPO_4$, SiO_2
(C) 640 °C/15 min	$Na_2Ca_4(PO_4)_2SiO_4$	(C) 600 °C/1 min	$NaCaPO_4$, SiO_2
(D) 700 °C/8 h	FAP	(D) 650 °C/1 min	$Na_2Ca_4(PO_4)_2SiO_4$, FAP
(E) 850 °C/1 h	FAP	(E) 700 °C/1 min	$Na_2Ca_4(PO_4)_2SiO_4$, FAP
(F) 1050 °C/1 h	FAP	(F) 750 °C/1 min	$Na_2Ca_4(PO_4)_2SiO_4$, FAP
		(G) 800 °C/1 min	FAP
		(H) 850 °C/1 min	FAP
		(I) 900 °C/1 min	FAP

around these nuclei, and (3) the origin and identity of intermediate phases formed during the crystallization process at various annealing temperatures. To answer these questions and to elucidate the crystallization mechanism in more detail, the use of complementary structural and analytical techniques is essential. In particular, solid-state NMR techniques appear promising, due to their well-proven ability to provide a wealth of local structural information on disordered materials and glasses.[3] The advantageous spectroscopic features of NMR, its element selective and inherently quantitative character, make it a particularly useful tool for the study of compositionally complex systems such as the present one, where the apatitic component of interest is only a minor constituent. In recent years, incisive third-generation NMR experiments have been developed, facilitating structural assignments and spectral editing on the basis of internuclear dipole−dipole interactions, measured under high-resolution conditions with the help of special double-irradiation techniques.[4,5] Such techniques have already been applied to the study of medium-range order in glass-forming systems and ceramics of great variety.[6−13] In the present study we describe the first application of multinuclear single- and double-resonance solid-state NMR techniques to the field of bioceramics. The results are discussed in the light of previous experimental evidence, providing a clearer picture of the crystallization mechanism.

Experimental Section

Sample Preparation and Characterization. Glass with the composition (mol %) 61.5 SiO_2−9.4 Al_2O_3−9.2 Na_2O−7.7 K_2O−6.0 CaO−1.9 P_2O_5−2.5 F−0.2 TiO_2−0.3 CeO_2−0.5 Li_2O−0.3 B_2O_3 was melted at 1480 °C for 1 h and 40 min and cast into monolithic blocks of approximately 1 × 2 × 10 cm. After cooling of the melt, the glass blocks were cut into smaller monolithic bodies, and their nucleation and crystallization properties were studied within two series by different heat-treatment protocols, summarized in Table 1. Samples of series I were thermally treated as frits and subsequently pulverized. The characterization of the resulting products has been described in detail in the literature.[2] Samples of series II were prepared by rapid compression of the glassy melt into disks (quenching rate 800 K/min) and subsequent heating to the desired temperature at a rate of 1 K/min. X-ray powder diffraction (XRD) data were obtained on a Bruker-AXS diffractometer D5005 operating with a Cu anode (λ = 1.540 56 Å). Measurements were recorded in the $\theta-\theta$ configuration at a scan rate of 0.0145 deg/s. Differential thermal analysis data were obtained on a NETZSCH STA 409 apparatus, using a heating rate of 10 K/min.

Solid-State NMR. ^{31}P solid-state NMR spectra were collected in the single-pulse mode at 202.5 MHz, using a Bruker Avance DSX-500 spectrometer equipped with a 4 mm MAS NMR probe, providing sample spinning rates near 12 kHz. Data were acquired with 90° pulses of 4 μs length and 64 scans with a repetition time of 10 s. Chemical shifts are reported relative to 85% H_3PO_4. ^{19}F MAS NMR spectra were acquired on a Bruker DSX-500 spectrometer, at 188.3 MHz in a 4.65 T magnet. Samples were spun within 4 mm rotors at spinning frequencies of 10−15 kHz. To suppress ^{19}F background signals, the DEPTH pulse sequence[14] was used. The 90° pulse length in these experiments was 4.5 μs. A total of 320−640 scans were acquired with a relaxation delay of 5 s. Experiments using longer relaxation delays (up to 200s) were conducted to ensure that the spectra obtained under the above-reported conditions yielded representative results. Chemical shifts are externally referenced to $CFCl_3$. Supplemental ^{23}Na and ^{29}Si NMR characterization of the samples on the DSX-500 spectrometer showed no interesting annealing effects in either series. The ^{23}Na MAS NMR spectra are characterized by a broad asymmetric resonance centered near −10 ppm vs 1 M aqueous NaCl solution. The spectra show no distinct sharp features characteristic of well-crystallized materials. Similar observations were made in the ^{29}Si MAS NMR spectra, recorded at 12 kHz spinning speed with a relaxation delay of 15 min. Invariably, these spectra show broad resonances centered near −94 ppm with a line width of 15 ppm, as typically observed for amorphous materials. Finally, ^{27}Al MAS NMR spectra obtained on representative samples indicate aluminum to be predominantly four-coordinated (asymmetric resonance with a peak maximum near 50 ppm vs 1 M aqueous $AlCl_3$ solution).

To probe for the presence and strength of heteronuclear dipole−dipole couplings, the pulse sequences REDOR (rotational echo double resonance)[4] and TRAPDOR (transfer of populations with double resonance)[5] were used. The pulse sequences are shown in Figure 1. The heterodipolar coupling between the nuclear spin species S (whose signal is detected) and spatially close nuclear spin species I is normally averaged away by MAS; however, it can be reintroduced into the experiment by coherent I-spin irradiation during the rotor period. In an $S\{I\}$ REDOR experiment this is accomplished by applying π-pulses on the I channel in the middle of the rotor period, whereas $S\{I\}$ TRAPDOR experiments utilize continuous-wave irradiation at the I-spin resonance. If heteronuclear dipole−dipole interactions are present, the I-spin irradiation causes a decrease in S-spin signal intensity, relative to a reference experiment without I-spin irradiation (intensity S_0).

(3) Eckert, H. *Prog. NMR Spectrosc.* **1992**, *24*, 159.
(4) Gullion, T.; Schaefer, J. S. *J. Magn. Reson.* **1989**, *81*, 196.
(5) Grey, C. P.; Vega, A. J. *J. Am. Chem. Soc.* **1995**, *117*, 8232.
(6) Van Wüllen, L.; Züchner, L.; Bertmer, M.; Eckert, H. *Ber. Bunsen-Ges. Phys. Chem.* **1996**, *100*, 1539.
(7) van Wüllen, L.; Züchner, L.; Müller-Warmuth, W.;. Eckert, H. *Solid State Nucl. Magn. Reson.* **1996**, *6*, 203.
(8) Rong, C.; Wong-Moon, K. C.; Li, H.; Hrma, P.; Cho, H. *J. Non-Cryst. Solids* **1998**, *332*, 32.
(9) Chan, J. C. C.; Bertmer, M.; Eckert, H. *Chem. Phys. Lett.* **1998**, *292*, 154.
(10) Bertmer, M.; Chan, J. C. C.;. Eckert, H. *J. Am. Chem. Soc.* **1999**, *121*, 5238
(11) Bertmer, M.; Züchner, L.; Chan, J. C. C.; Eckert, H. *J. Phys. Chem. B* **2000**, *104*, 6541.
(12) Prabakar, S.; Wenslow, R. M.; Mueller, K. T. *J. Non-Cryst. Solids* **2000**, *82*, 263.
(13) van Wüllen, L.; Eckert, H.;.Schwering, G. *Chem. Mater.* **2000**, *12*, 1840.
(14) Cory, D. G.; Ritchey, W. M. *J. Magn. Reson.* **1988**, *80*, 128

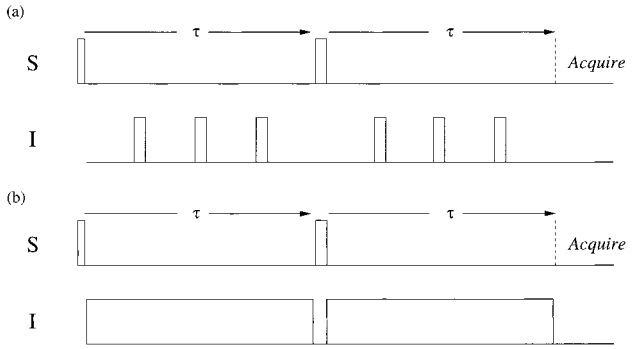

Figure 1. NMR pulse sequences used in the present study: (a) rotational echo double resonance (REDOR); (b) transfer of populations with double resonance (TRAPDOR).

Table 2. Experimental Conditions Used in the Double-Resonance NMR Experiments

combination	^{31}P{^{23}Na}	^{31}P{^{19}F}	^{19}F{^{31}P}	^{19}F{^{27}Al}	^{19}F{^{23}Na}
expt	TRAPDOR	REDOR	REDOR	TRAPDOR	TRAPDOR
ν_r (kHz)[a]	12	30	30	30	30
$\nu_o(S)$ (MHz)[b]	202.5	202.5	470.5	470.5	470.5
$\nu_o(I)$ (MHz)[c]	132.3	470.5	202.5	130.3	132.2
$\tau_{90°}(S)$ (μs)[d]	6.0	3.5	6.0	6.0	6.0
$\tau_{90°}(I)$ (μs)[e]	3.0	6.0	3.5	12.0	7.0
T_D (ms)[f]	variable	1.6	1.6	1.0	2.0
T_R (s)[g]	10	10	5.0	5.0	5.0

[a] MAS rotor frequency. [b] *S* -spin resonance frequency. [c] *I*-spin resonance frequency. [d] *S*-spin-90° pulse length. [e] *I*-spin-90° pulse length. [f] Dephasing delay. [g] Relaxation delay.

The magnitude $(S_0 - S)/S_0$ of the difference signal depends on both the strength of the dipole−dipole coupling and on the length NT_r (number of rotor cycles times duration of one rotor period) of the overall dipolar evolution time. REDOR experiments lend themselves to a more straightforward quantitative analysis whereas TRAPDOR experiments are more effective (and thence preferred) in the case of quadrupolar *I* nuclei. Table 2 gives a summary of the various double resonance experiments carried out and the specific conditions used. ^{31}P{^{23}Na} and ^{31}P{^{27}Al} TRAPDOR studies were conducted in a 4 mm ^{31}P−X double-resonance probe while all the double-resonance experiments involving ^{19}F nuclei utilized a 2.5 mm double-resonance probe.

Results, Assignments, and Interpretation

XRD and DTA Results. Figure 2 shows the XRD results for the two series investigated. The crystalline phases detected by X-ray powder diffraction are listed in Table 1. For both series, the formation of FAP is preceded by the appearance of crystalline precursor phases. In series I, the formation of FAP by heat treatment at 700 °C for 8 h is essentially quantitative. With the shorter annealing times employed in the heating protocol of series II, the required temperature for quantitative FAP formation is 800 °C. In both series, the *d* values observed for FAP are found systematically shifted to those of the reference phases, suggesting some deviation from perfect stoichiometry.

It is interesting to note that the precursor phases formed by annealing at temperatures <750 °C appear to be different for the two series. For samples IIA−C, the XRD powder pattern shows an excellent match with a diffractogram published for $NaCaPO_4$, JCPDS No. 29-1193; in addition traces of SiO_2 (quartz) are detectable. For samples IID,E, a significant decrease in resolution is observed, and a reasonable match can be found to a pattern published for a phase of composition

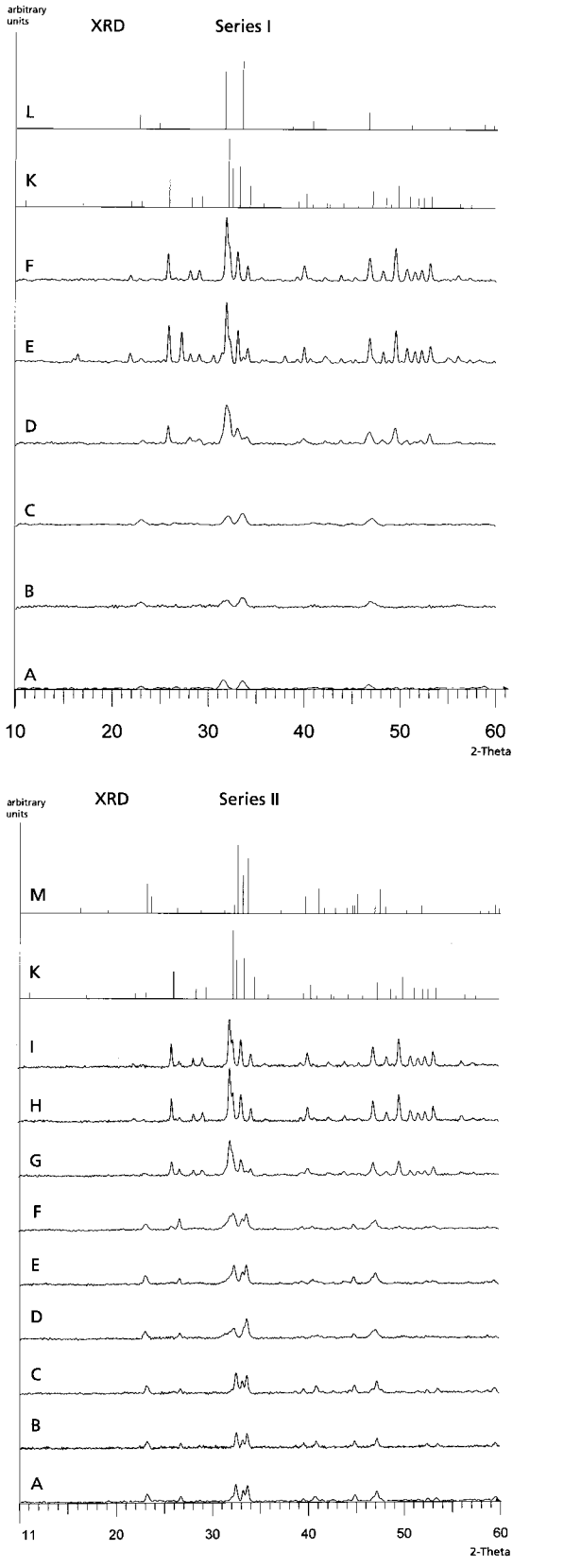

Figure 2. X-ray powder diffraction results obtained on samples of series I and II. See Table 1 for the notations of series IA−F and IIA−I, respectively. Traces K−M show the expected XRD powder patterns of crystalline FAP, $NaCaPO_4$, and $Na_2Ca_4(PO_4)_2SiO_4$, respectively.

$Na_2Ca_4(PO_4)_2SiO_4$, JCPDS No. 33-1229. However, characteristic lines of $NaCaPO_4$ are still observed, suggesting that this phase is still present to some extent. For

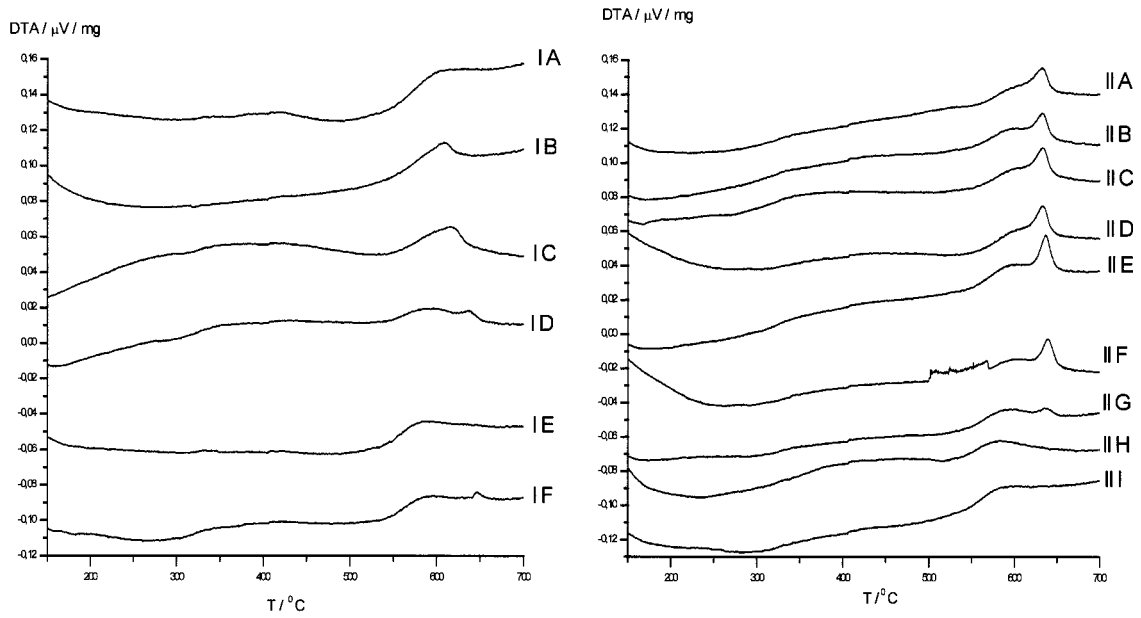

Figure 3. Differential thermal analysis results obtained on samples of series I and II. The individual traces have been offset for clarity.

Table 3. ^{19}F NMR Chemical Shifts Observed and Assignments

$\delta(^{19}F)$/ppm	assgnt	samples obsd
−104	FAP	ID−F, IIF,I
−130 ± 10	F (Na, Ca, K, P) in glassy phase	IA−C, IIA−F
−190 ± 10	F (Al) (second glassy phase)	IA−F, IIA−H

samples IA−C, the powder patterns show diffraction lines at *d* values similar to those observed in sample IID. Again, the best match was found to a pattern published for a phase of composition $Na_2Ca_4(PO_4)_2SiO_4$, JCPDS No. 33-1229. In samples ID−H and IIF−I (which were treated at temperatures at or above 700 °C) the powder patterns are dominated by the diffraction lines of FAP. Thus, the XRD data suggest the absence of $NaCaPO_4$ in samples of series I.

Figure 3 shows the corresponding DTA data for both series. For most samples of series I, no thermal events can be noticed aside from the glass transition point near 550 °C associated with the softening of the glass matrix. This result stands in sharp contrast to those reported in refs 1 and 2, whereas the thermal analysis data for samples II A−G reproduce the marked endotherms near 640 °C that were previously reported. Finally the endotherm is absent in samples IIH,I where FAP is crystallized. In conjunction with the XRD data, our results indicate that the presence of this endotherm is closely related to the formation of $NaCaPO_4$ as an intermediate phase in apatite crystallization. Obviously, the mechanisms of apatite crystallization are different between series I and II, respectively.

^{19}F MAS NMR. Figure 4a,b shows the single-resonance ^{19}F MAS NMR spectra of both series of samples. Spectral parameters extracted from these data are summarized in Table 3. For all of the samples annealed below 700 °C the ^{19}F MAS spectra consist of two broad peaks centered near −130 and −190 ppm, respectively. The line widths of these peaks (in Hz) are independent of the MAS-spinning speed and increase with increasing field strength, indicating that they are dominated by a distribution of isotropic chemical shifts. Such shift distributions indicate a continuous variation in chemical environments as they are typical for the glassy state. Therefore, Figure 4a,b suggests that the entire fluorine inventory remains in the amorphous state for these samples. Extended annealing at 700 °C or above results in the formation of FAP, as clearly revealed by the appearance of a sharp resonance at −104 ppm (see spectra of series I).[15] Small quantities of FAP are also detectable in samples ramped up to 700 °C (series II); however, the fraction of fluorine present in this form remains small (see Figure 4b). At the heating rate of 1 K/min used, a maximum temperature of 800 °C appears to be necessary to convert the majority of fluorine into the crystalline FAP form. Furthermore, both the extended annealing and the ramping experiments indicate that the two fluorine populations detected in the amorphous state are depleted at different rates, and at least part of the ^{19}F signal at −190 ppm persists up to the highest annealing temperature. This result suggests that both of the glassy microphases contain fluorine, giving rise to the broad signals detected in samples IA−C and IIA−F, respectively. This conclusion is further supported by the double-resonance NMR experiments discussed below.

^{19}F{^{31}P}, ^{19}F{^{27}Al}, and ^{19}F{^{23}Na} Double-Resonance NMR. To facilitate the assignments of the ^{19}F NMR signals observed in the single-pulse experiments, a variety of spectral editing studies were undertaken on the glassy samples of series I, by probing heterodipolar interactions with ^{31}P, ^{27}Al, and ^{23}Na via REDOR or TRAPDOR experiments. These results are summarized in Figure 5. In each individual trace, the upper curve represents the ^{19}F single-resonance signal, whereas the bottom curve shows the signal acquired following irradiation of the respective heteronuclei in the middle of the rotor period. Significant signal attenuation observed in the latter experiment indicates the presence of substantial dipolar couplings, revealing spatial prox-

(15) Braun, M.; Hartmann, P.; Jana, C. *J. Mater. Sci.: Mater. Med.* **1995**, *6*, 150.

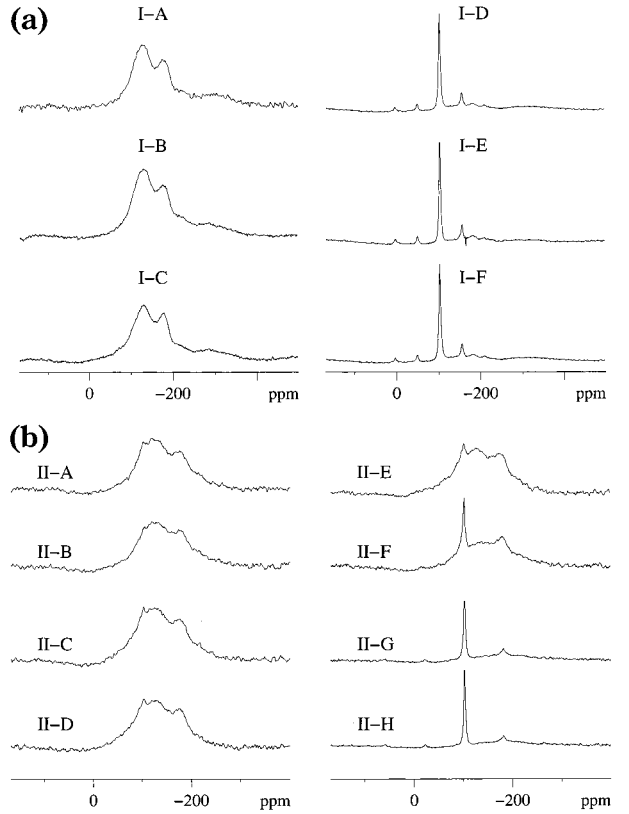

Figure 4. ^{19}F single-pulse MAS NMR spectra of the samples under study: (a) series I; (b) series II.

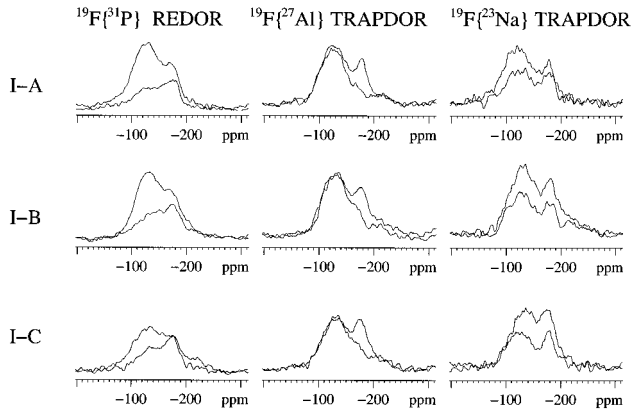

Figure 5. Double-resonance NMR studies carried out with ^{19}F observation on representative samples of series I: left, $^{19}F\{^{31}P\}$ REDOR; middle, $^{19}F\{^{27}Al\}$ TRAPDOR; right, $^{19}F\{^{23}Na\}$ TRAPDOR. In each individual trace, the upper curve represents the ^{19}F single-resonance signal, whereas the bottom curve shows the signal acquired following irradiation of the respective heteronuclei during the rotor period.

imity. Thus the $^{19}F\{^{31}P\}$ REDOR data for samples IA,B reveal that the −130 ppm component is substantially reduced by ^{31}P irradiation, indicating that these ^{19}F species are in close proximity of phosphorus. In contrast, the −190 ppm signal is hardly affected in this experiment, indicating the corresponding species to be remote from phosphorus. Figure 5, middle, shows the complementary data from $^{19}F\{^{27}Al\}$ TRAPDOR. These results indicate unambiguously that only the fluorine sites giving rise to the −190 ppm component strongly interact with the ^{27}Al nuclei. Inspection of the ^{19}F solid-state chemical shift database[16] provides additional support for this assignment. Furthermore, Figure 5, right, indicates that both of the fluorine species are in the proximity of sodium ions and interact with them equally strongly. Overall the results of the double-resonance NMR studies lend strong support to the interpretation that the two fluorine species occur in two distinct glassy phases. One phase contains the entire phosphorus inventory, and the other one contains the entire aluminum inventory of the samples studied. Sodium appears to be present in both of the phases.

Table 4. ^{31}P NMR Chemical Shifts δ (±0.1 ppm), Linewidths Δ (±10%) Observed, and Assignments

$\delta(^{31}P)$/ppm	Δ/ppm	assgnt	samples obsd
4.9	7.8	glassy phase	IA−C, IIA−E
2.8	3.5	$NaCaPO_4$	IIA−C
3.3	3.0	$Na_2Ca_4(PO_4)_2SiO_4$	IA−C, IID−E
3.8	4.0	FAP	ID−H, IIG,I

Finally, Figure 5 indicates that the magnitude of the $^{19}F\{^{31}P\}$ REDOR effect observed for the −130 ppm resonance attributed to ^{19}F in the glassy phase tends to decrease in going from sample IA to IC, i.e., as the annealing temperature of the samples is increased. The effect is much less apparent in the $^{19}F\{^{23}Na\}$ and the $^{19}F\{^{27}Al\}$ TRAPDOR data. This observation will be discussed in conjunction with the ^{31}P MAS NMR results in more detail below.

^{31}P MAS NMR. Figure 6a,b shows the single-resonance ^{31}P MAS NMR spectra of both series of samples. Spectral parameters extracted from these data by detailed line shape deconvolution are summarized in Table 4. For the series-I glasses, the ^{31}P MAS spectra reveal an increase in crystallinity as the temperature and duration of the annealing step are successively increased. In sample IA the phosphorus component appears still to be largely amorphous (peak position 4.9 ppm), as revealed the fairly large line width of 7.8 ppm. The spectra of samples IB,C reveal two distinct ^{31}P environments, deconvoluted into an amorphous component at 4.9 ppm and a crystalline component at 3.3 ppm, which is assigned to $Na_2Ca_4(PO_4)_2SiO_4$ on the basis of the XRD data. Finally, samples ID−G show a single ^{31}P site, corresponding to that in crystalline $Ca_5(PO_4)_3F$ (FAP). The isotropic chemical shift value of 3.8 ppm is consistent with that reported for fluoroapatite (FAP).[17] Results on the series II glasses are essentially similar; however, they reveal a generally larger degree of crystallinity of the phosphorus component at the lower annealing temperatures. This is confirmed by the X-ray powder diffraction results, which reveal the presence of well-crystallized $NaCaPO_4$ in samples IIA−C. The corresponding ^{31}P chemical shift is 2.8 ppm. An interesting anomaly is observed in sample IID (annealing temperature 650 °C), which reveals a minimum in crystallinity both in the NMR and the XRD experiments. At the same time the sharp ^{31}P signal component shifts to 3.3 ppm. This finding confirms an earlier report, where the change in the XRD powder pattern observed was attributed to a phase transformation (also detected by DTA), resulting in the formation of a new phase ("X-phase").[2] Note that although the single-pulse ^{31}P MAS NMR technique provides very little overall spectroscopic resolution, it is still possible to differenti-

(16) Miller, J. M. *Prog. NMR Spectrosc.* **1996**, *28*, 255.
(17) Rothwell, W. P.; Waugh, J. S.; Yesinowski, J. P. *J. Am. Chem. Soc.* **1998**, *102*, 2637.

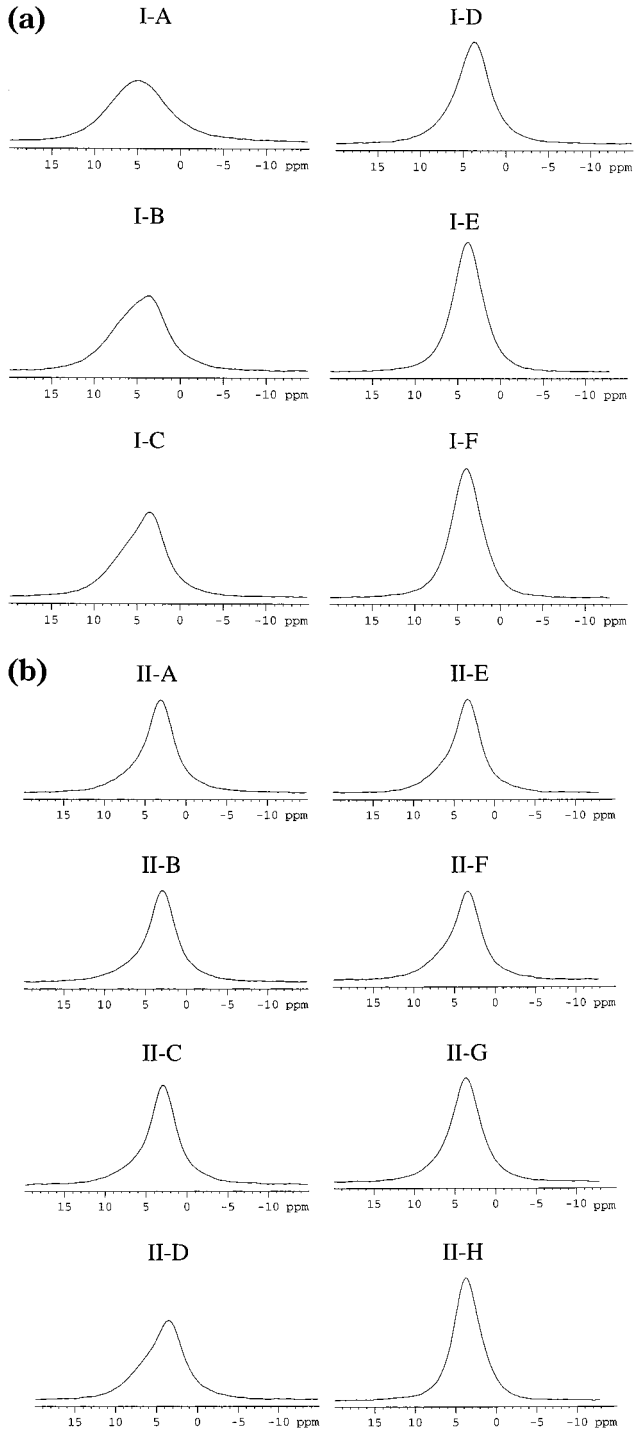

Figure 6. ^{31}P single-pulse MAS NMR spectra of the samples under study: (a) series I; (b) series II.

ate between the ^{31}P chemical shifts of the precursor phases glass, $Na_2Ca_4(PO_4)_2SiO_4$, and $NaCaPO_4$ by detailed peak deconvolution. In particular, the ^{31}P NMR chemical shift trends support the idea of a phase transformation in going from sample IIC to IID. Both the XRD and the NMR results suggest that the crystalline precursor phase formed in sample IID is identical to that present in samples IA−C.

^{31}P{^{23}Na} TRAPDOR NMR. Figure 7 shows ^{31}P{^{23}Na} TRAPDOR results on all of the samples. In each trace, the upper curve represents the ^{31}P signal without ^{23}Na irradiation, whereas the lower curve is the signal obtained in the experiment conducted with

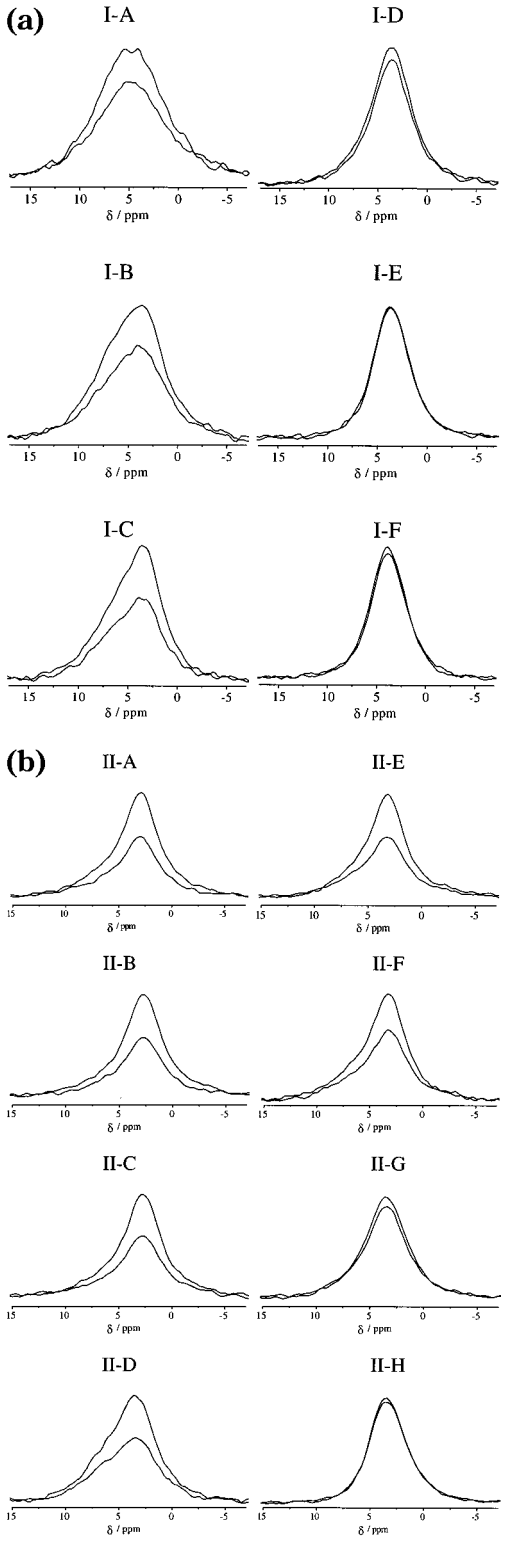

Figure 7. ^{31}P{^{23}Na} TRAPDOR NMR results obtained on representative samples of series I and II. In each trace, the upper curve represents the ^{31}P signal without ^{23}Na irradiation, whereas the lower curve is the signal obtained in the experiment conducted with irradiation of the sodium resonance during the rotor period.

irradiation of the sodium resonance during the rotor period. These results reveal unambiguously that in samples IA−C and IIA−F there is a significant ^{31}P−^{23}Na dipolar interaction (as expected in both $Na_2Ca_4(PO_4)_2SiO_4$ and $NaCaPO_4$), whereas in samples ID−G and IIG−I the identical ^{31}P NMR signal intensities

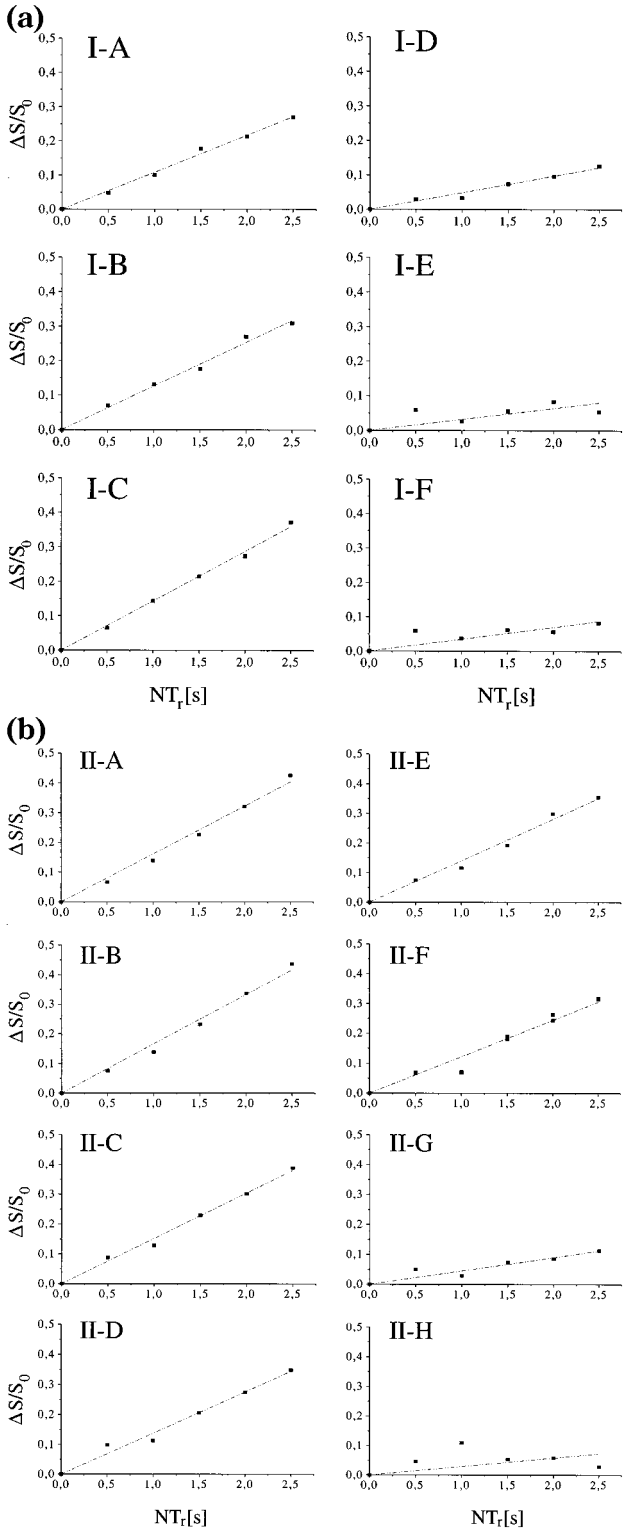

Figure 8. $^{31}P\{^{23}Na\}$ TRAPDOR dephasing curves (plot of normalized intensity of the difference signal versus dipolar evolution time) obtained on representative samples of series I and II.

observed in the experiments with and without ^{23}Na irradiation indicate that crystallization of the phosphorus inventory to sodium-free FAP is essentially quantitative. These results are in excellent agreement with the XRD data. More quantitative insight can be obtained on the basis of the corresponding TRAPDOR dephasing curves summarized in Figure 8. Since all of the TRAPDOR curves were obtained under identical

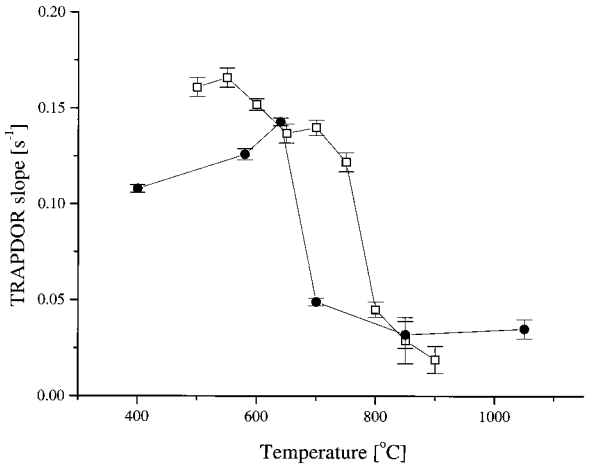

Figure 9. $^{31}P\{^{23}Na\}$ TRAPDOR slopes plotted against sample annealing temperatures in series I and II. Filled circles refer to samples of series I, and open squares to samples of series II.

experimental conditions, the slopes determined from the plot of $\Delta S/S_0$ versus evolution time are a relative measure of the fraction of the phosphorus interacting with sodium. Figure 9 illustrates interesting dependences of these slopes on the annealing temperatures for both series studied. For series I, the $^{23}Na-^{31}P$ interaction strength initially increases as a function of annealing temperature. According to XRD and ^{31}P MAS NMR the crystallinity increases as a function of annealing temperature; consequently, the TRAPDOR result demonstrates that ^{31}P and ^{23}Na interact more strongly in the crystalline precursor phase $Na_2Ca_4(PO_4)_2SiO_4$ than in the parent glassy phase. The TRAPDOR slopes measured for samples IIA−C originate mostly from the $NaCaPO_4$ constituent. The TRAPDOR slopes measured in these samples (as compared to samples IA−C) are larger than those measured in samples of series I and also larger than those measured in samples IID,E. Furthermore, the TRAPDOR slopes measured in samples IID,E (attributed to $Na_2Ca_4(PO_4)_2SiO_4$ plus residual glass) are essentially identical to that measured in sample IC, and this resemblence agrees very well with the similarities observed in the corresponding XRD patterns and the ^{31}P MAS NMR spectra. Finally, for both series, the appearance of FAP as an annealing product results in abrupt decreases of the TRAPDOR slopes to significantly smaller values. In all of these materials the TRAPDOR effects still lie somewhat above the value of zero expected for pure FAP samples. This effect may indicate that some Na is incorporated into the FAP structure and/or some of the residual glassy matrix is still present.

$^{31}P\{^{19}F\}$ REDOR NMR. The proximity of ^{31}P and ^{19}F nuclei is addressed by the $^{31}P\{^{19}F\}$ REDOR experiments. Figure 10 summarizes the results obtained for samples of series I. Dipolar coupling of substantial magnitude is already detected in sample IA, indicating that P and F are joint components in at least one of the two separate phases of the initial glass. Samples IB and especially IC reveal a noticeable decrease in the $^{31}P-^{19}F$ interaction strength, consistent with the increasing dominance of the fluorine-free crystalline precursor phase $Na_2Ca_4(PO_4)_2SiO_4$ in these two samples. Nevertheless, the results indicate that not the entire

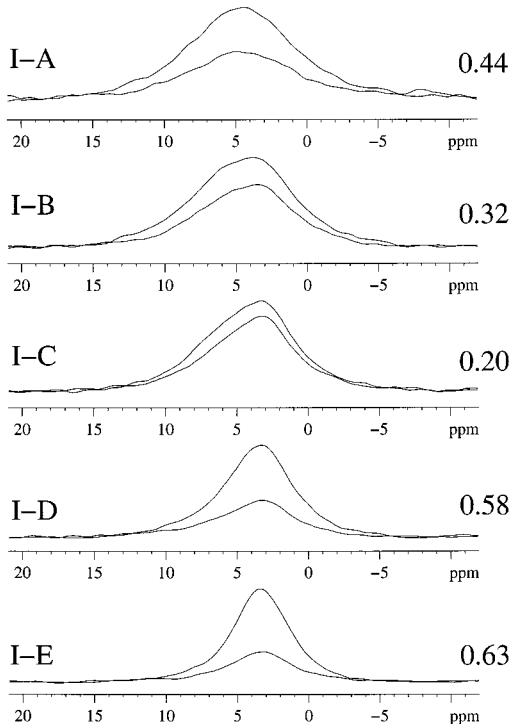

Figure 10. $^{31}P\{^{19}F\}$ REDOR NMR results obtained on representative samples of series I. In each trace, the upper curve represents the ^{31}P signal without ^{19}F irradiation, whereas the lower curve is the signal obtained in the experiment conducted with π pulses on the ^{19}F channel during the rotor period. Numerals indicate REDOR fraction $(S_0 - S)/S_0$ measured for a dipolar evolution time $T_D = 1.6$ ms.

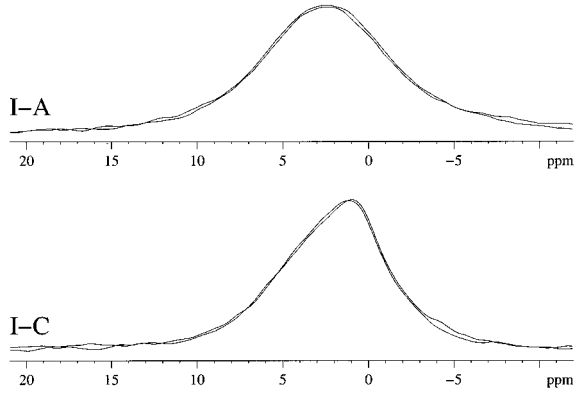

Figure 11. $^{31}P\{^{27}Al\}$TRAPDOR NMR results obtained on two representative samples. In each plot, the two traces correspond to the ^{31}P NMR signal with and without resonant CW irradiation of the ^{27}Al nuclei. Note the absence of any signal attenuation in both samples.

P-component is crystallized at these annealing stages. Finally, in samples ID,F, the $^{31}P-^{19}F$ dipolar interaction strength is seen to increase again, consistent with the dominant formation of FAP in these samples. The detailed $^{31}P \leftrightarrow ^{19}F$ REDOR characterization of crystalline FAP has been published previously[18] and is thus not the subject of the present contribution.

$^{31}P\{^{27}Al\}$ TRAPDOR NMR. Dipolar interactions between the ^{31}P and ^{27}Al nuclei have been probed by $^{31}P\{^{27}Al\}$ TRAPDOR NMR experiments. Figure 11 shows the results obtained on samples IA,C, using a 12 kHz spinning frequency and a dipolar evolution time of 2.0 ms. Within experimental error, no dipolar interaction is detectable between these spin species. This result supports the conclusion that phosphorus and aluminum reside in separate microphases, both in the glassy precursor and in the material resulting from annealing.

Discussion and Conclusions

The NMR results lend support to the crystallization model previously proposed and provide significant additional information. They confirm primary crystallization of fluorine-free sodium calcium phosphate-based precursor phases, as previously indicated from X-ray powder diffraction.[2] Detailed comparison of the results obtained for series I and series II indicates that the crystallization mechanism can be influenced by the thermal histories of these materials. In series I, the precursor phase is tentatively assigned to $Na_2Ca_4(PO_4)_2SiO_4$. In series II, $NaCaPO_4$ is formed initially, followed by at least partial phase transformation to $Na_2Ca_4(PO_4)_2SiO_4$, which is accompanied by some loss of crystallinity. This phase transformation gives rise to an endotherm near 640 °C as revealed by DTA. Subtle differences in the ^{31}P chemical shifts of these phases can be detected by ^{31}P MAS NMR at sufficiently high magnetic field strength (11.7 T). Additional details are revealed by the double-resonance NMR results, which indicate a strong $^{31}P-^{23}Na$ dipolar coupling in the crystalline precursor phases, weaker interactions in the parent glass, and no interaction (as expected) in the final FAP product. Furthermore, it is clear that the crystalline fluorine-free precursor phase forms from the amorphous droplet phase, which contains the elements sodium, calcium, and phosphorus as well as the larger part of the fluorine inventory (signal near −130 ppm). Within the series IA−C, the gradual decrease of the $^{31}P-^{19}F$ dipolar coupling strength with increasing annealing temperature, evident from both the $^{19}F\{^{31}P\}$ and the $^{31}P\{^{19}F\}$ REDOR data, indicates that the fraction of P present as $Na_2Ca_4(PO_4)_2SiO_4$ increases at the expense of phosphorus in the amorphous state. At the same time, fluorine is retained in the amorphous state and remains unaltered by this treatment. The reversible thermal event (the endotherm in the DTA heating curve) observed near 640 °C is clearly linked to the presence of $NaCaPO_4$ and attributed to a phase transformation $NaCaPO_4 \rightarrow Na_2Ca_4(PO_4)_2SiO_4$. Presumably the latter material is the "X-phase" previously suggested to occur in samples annealed at temperatures >640 °C. While the NMR results clearly confirm the existence of a precursor phase with an identity different from $NaCaPO_4$, the compositional assignment to $Na_2Ca_4(PO_4)_2SiO_4$ must still be considered tentative at this stage. As a matter of fact, the ^{29}Si MAS NMR spectra of samples presumed to contain this phase show no evidence for it. Neither do the spectra reveal any significant intensity near −80 ppm (where $Q^{(0)}$ resonances are expected), nor do they contain any sharp peaks attributable to crystalline phases. On the other hand, owing to the low P-content of the samples, the phase $Na_2Ca_4(PO_4)_2SiO_4$ would constitute only a very minor fraction (maximum 1%) of the silicon inventory, which may be too difficult to detect because of dynamic range problems and/or long relaxation times. Similar reasons may explain that the NMR spectra also proved unable

(18) Pan, Y. *Solid State Nucl. Magn. Reson.* **1995**, *5*, 263.

to substantiate the formation of quartz, the presence of which was also suggested from the XRD data.

As the results obtained on series I indicate, FAP is only formed after annealing the sample at 700 °C for 8 h. For samples in series II, the duration of heat treatment at 700 °C was insufficient to convert the bulk of the sample into FAP and thus even higher temperatures are required to accomplish this with the heating protocol used here. We suspect that the high temperatures are necessary to attain a sufficiently low viscosity of the remaining glassy droplet phase to facilitate transport of fluoride to the sodium calcium phosphate clusters, resulting in FAP formation via a diffusion-controlled reaction. The dramatic change observed in the ^{19}F NMR spectra of series I and II is entirely consistent with the observation of FAP as the dominant phase present in the XRD powder patterns of such samples.[2] Still, both the observation of the 640 °C endotherm and the nonzero $^{31}P\{^{23}Na\}$ TRAPDOR effects in samples annealed as high as 900 °C/min (sample II-I) suggests that part of the droplet phase remains in the amorphous state under these conditions. Also, the residual ^{19}F resonance (near −190 ppm) observed in such high-annealed samples indicates that part of the fluorine inventory (i.e. largely the species interacting with Al) remains in the amorphous state, most likely the glassy matrix phase. This latter result is not unexpected, since the F/P ratio of the batch composition (2.5/3.8) is higher than that of FAP (1/3), so that not all of the fluoride present can end up in the form of fluoroapatite. From the present results it is not clear whether this remaining fluoride species is at all involved in the FAP crystallization mechanism. Further insight into this question will come from in-situ high-temperature NMR studies, which are currently in progress.

Overall, the present study is the first report on the application of double-resonance NMR methods to the field of bioceramics. Owing to their sensitivity to local dipolar interactions, these element-selective methods can complement SEM and TEM techniques in elucidating the elemental distribution in phase-separated materials and, at the same time, provide valuable information about local environments. Further applications to other systems of biomedical interest are currently under investigation.

Acknowledgment. Financial support from the Deutsche Forschungsgemeinschaft (Grant Ec168/3-1) and by Ivoclar Co. is gratefully acknowledged. J.C.C.C. acknowledges a personal stipend from the Alexander-von-Humboldt Foundation.

CM0101834